ISSN 1029-9599, Physical Mesomechanics, 2022, Vol. 25, No. 6, pp. 557–567. © Pleiades Publishing, Ltd., 2022.
Russian Text © The Author(s), 2022, published in Fizicheskaya Mezomekhanika, 2022, Vol. 25, No. 4, pp. 94–105.

Three-Level Dislocation-Based Model for Describing the Deformation of Polycrystals: Structure, Implementation Algorithm, Examples for Studying Nonproportional Cyclic Loading

D. S. Gribov[1] and P. V. Trusov[1]*

[1] *Perm National Research Polytechnic University, Perm, 614990 Russia*
** e-mail: tpv@matmod.pstu.ac.ru, tpv@pstu.ru*

Received April 28, 2022; revised May 20, 2022; accepted May 22, 2022

Abstract—A three-level constitutive model is proposed for describing the deformation of polycrystalline materials, which is based on crystal elasto-viscoplasticity and the introduction of internal variables. The structure, mathematical formulation, and implementation algorithm of the model are discussed. The element of the upper structural-scale level is the representative macrovolume. The elements of mesolevels 1 and 2, which are identical in scale, are crystallites (grains, subgrains, fragments, depending on the required element size). The description at mesolevel 1 is performed in terms of thermomechanical variables (stresses, strains, strain rates). The behavior of meso-2 elements is described in terms of dislocation densities and velocities. Particular attention is paid to the formation of barriers on split dislocations. As an example, the model is applied to study proportional and nonproportional cyclic loading of samples with substantially different stacking fault energies. It is shown that barriers are more readily formed in materials with low stacking fault energy, leading to their additional cyclic hardening under nonproportional loading.

Keywords: multilevel model, split dislocations, hardening, dislocation barriers, nonproportional cyclic loading

DOI: 10.1134/S102995992206008X

1. INTRODUCTION

The need to control material properties in the production of metal and alloy structures requires the development and continuous improvement of constitutive models (constitutive equations) that can describe the evolution of physical and mechanical characteristics under widely variable thermomechanical loads. The existing models for studying the behavior of polycrystalline materials can be divided into macrophenomenological [1–9, etc.] and crystal plasticity ones [10–21, etc.]. Macrophenomenological models are usually formulated in the form of complex operators over loading history, and the parameters of these operators are determined by laborious full-scale tests (including multiaxial loading tests). The majority of models of this type do not consider, at least explicitly, meso- and microscopic physical processes that cause significant changes in the structure of materials. Taking into account various physical mechanisms of inelastic deformation, their interactions, and the complexity of their description in terms of continuum mechanics parameters, macrophenomenological constitutive relations provide good accuracy in the analysis of material behavior in narrow loading parameter ranges. In addition, such relations show higher computational efficiency in solving technological boundary value problems, which makes them attractive for the development of application software packages.

The mechanical properties of metals and alloys strongly depend on their meso- and microstructure. This is the reason for the rapid development of multiscale crystal plasticity models [22–25, etc.], which allow one to explicitly describe the evolving structure of materials. In contrast to the wide variety of macrophenomenological models, which usually describe the behavior of specific materials in narrow thermomechanical load ranges, multiscale crystal

plasticity models are more versatile. Despite the huge diversity of multilevel models proposed in the literature, there are insufficiently studied issues of complex loading processes or the effect of some features of the defect structure on the behavior of alloys, e.g., the presence of stacking faults (dislocation splitting). Here we use an approach that involves internal variables [26–31] characterizing the meso- and microstructure of the material and included in the structure of the constitutive model of evolution equations to describe their change. The developed model belongs to the class of three-level statistical models. The structure, implementation algorithm, and some results of applying the dislocation-based model are discussed. Numerical experiments are conducted on a representative macrovolume of a polycrystalline material, which can be loaded in the same way as macrosamples in full-scale experiments. Particular attention is paid to the analysis of the influence of the stacking fault energy on the behavior of polycrystalline samples under nonproportional cyclic loading.

2. CONCEPTUAL AND MATHEMATICAL FORMULATIONS OF THE MODEL

The developed model belongs to the family of statistical models and includes submodels for describing the behavior of polycrystals at three structural-scale levels: macrolevel, which describes the response of a representative macrovolume; mesolevel 1, which describes the behavior of crystallites (subgrains, fragments) in terms of mechanical variables (stresses, strains, etc.); and mesolevel 2, which considers the evolution of defect densities for dislocations, dislocation loops, and barriers formed during the interaction of split dislocations. As noted above, the model is based on an approach where explicit and implicit internal variables are introduced at each level. These are tensor-valued (arbitrary rank) variables that describe the evolving meso- and microstructure of lower levels. The introduction of the additional variables eliminates the use of complex operator (functional) equations in constitutive models, while it remains possible to account for the memory of the material carried by the internal variables. Most of the constitutive model equations in this case are tensor-algebraic or ordinary differential equations. It is assumed that the internal variables are homogeneous within the considered elements of a given level. Explicit internal variables enter directly into the constitutive relations of the given level. They are related by kinetic equations with implicit variables that describe the structure of the material at deeper structural-scale levels [30].

The representative macrovolume contains a set of grains. Each grain includes a statistically significant set (tens or hundreds) of crystallites (subgrains, fragments), or meso-1 elements, which have a slight misorientation within individual grains in the reference configuration (Fig. 1). Meso-1 elements are identical in scale to meso-2 elements, but the behavior of materials at these levels is described in terms of different variables. The description at the macrolevel and mesolevel 1 is carried out in terms of mechanical variables (stresses, strains, strain rates), and at mesolevel 2 the model operates with the densities of various defects on slip systems.

The explicit internal variables at the level of the representative macrovolume include the tensors of the inelastic part of the strain rate, elastic characteristics, and the spin (macroscopic variables). At mesolevel 1, these are the tensors of the elastic properties of the crystallite, the inelastic part of the strain rate, and the spin; the implicit variables are the shear rates on slip systems, critical shear stresses, dislocation densities and velocities on slip systems. All internal variables at mesolevel 2 (except temperature) are determined on the introduced slip systems: the explicit internal variables include the critical stresses on slip systems, average dislocation velocities and dislocation densities; the implicit variables are the dislocation barrier and source densities on slip systems.

In the adopted Voigt hypothesis (implying the equality of velocity gradients at the macrolevel and mesolevel 1), the velocity gradient tensor components are transferred from macrolevel to mesolevel 1

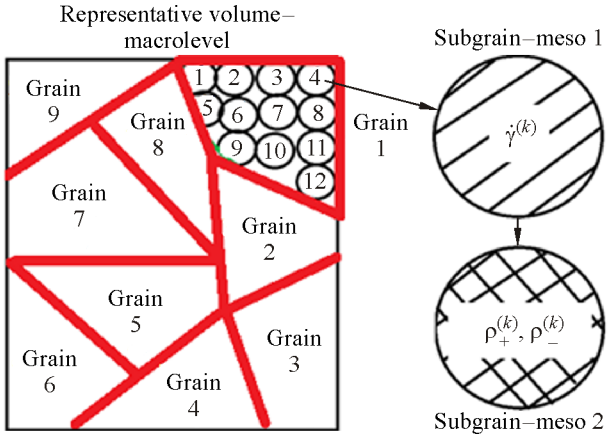

Fig. 1. Schematic illustration of the model structural-scale levels: representative macrovolume of polycrystalline material, grain, subgrain.

as impacts, and the deformation process is described in terms of mechanical variables. The actual stresses used to determine the shear stresses on slip systems are transferred from mesolevel 1 to mesolevel 2, which are then used to calculate the dislocation velocities. At mesolevel 2, we describe the defect density evolution and determine changes in the critical stresses and average edge dislocation velocities, after which the Orowan equation is used to find the shear rates and transfer them to mesolevel 1. At mesolevel 1, we determine the inelastic part of the strain rate, lattice rotation, and the stress tensor components. The macroscopic stresses are determined by averaging over the set of meso-1 elements contained in the representative macrovolume.

The model is focused on describing the response (macroscopic stress tensor) of the representative macrovolume of a polycrystalline material (uniformly deformed macrosample) to a given kinematic load $\mathbf{Z} = \hat{\nabla}\mathbf{V}^{\mathrm{T}}$ ($\hat{\nabla}$ is the gradient operator defined in the current configuration). Applying the Voigt hypothesis, we determine the strain rate at mesolevel 1:

$$\mathbf{z}(t) = \mathbf{Z}(t), \tag{1}$$

where $\mathbf{z}$ is the velocity gradient at mesolevel 1. Hereinafter, the related mechanical characteristics of the macrolevel and mesolevel 1 are denoted by the same letters: capital letters for the macrolevel and lowercase for mesolevel 1.

For each meso-1 element, the plastic part of the strain rate is determined by the shear rates on slip systems (determined at mesolevel 2), after which the rate of change $\dot{\boldsymbol{\sigma}}$ of the Cauchy stress tensor $\boldsymbol{\sigma}$ is calculated from the additivity of the elastic and plastic parts of the strain rate:

$$\begin{gathered}\mathbf{z} = \mathbf{z}^{\mathrm{e}} + \mathbf{z}^{\mathrm{in}}, \\ \boldsymbol{\sigma}^{\mathrm{cr}} \equiv \dot{\boldsymbol{\sigma}} + \boldsymbol{\sigma}\cdot\boldsymbol{\omega} - \boldsymbol{\omega}\cdot\boldsymbol{\sigma} = \mathbf{\Pi} : (\mathbf{z} - \boldsymbol{\omega} - \mathbf{z}^{\mathrm{in}}),\end{gathered} \tag{2}$$

where $\mathbf{z}^{\mathrm{e}}$ and $\mathbf{z}^{\mathrm{in}}$ are the elastic and inelastic parts of the meso-1 strain rate, $\boldsymbol{\sigma}^{\mathrm{cr}}$ is the corotational derivative of the Cauchy stress tensor, $\mathbf{\Pi}$ is the 4-valence tensor of the elastic characteristics of the crystallite, and $\boldsymbol{\omega}$ is the spin of a rigid corotational frame (meso-1) associated with the lattice [32]. The rigid corotational frame is introduced to decompose the motion of deformable bodies into quasi-rigid and strain-induced ones [24]. The plastic part of the strain rate is determined using the Orowan equation by the shear rates $\dot{\gamma}^{(k)}$ calculated at mesolevel 2 (hereinafter the superscript k denotes the slip system number):

$$\mathbf{z}^{\mathrm{in}} = \sum_{k=1}^{n} \dot{\gamma}^{(k)} \mathbf{b}^{(k)} \mathbf{n}^{(k)}. \tag{3}$$

The relations for determining the spin tensor of a rigid corotational frame are given in [24, 32]. The spin tensor is related to the orientation tensor $\mathbf{o}$ of the rigid corotational frame by the equation

$$\boldsymbol{\omega} = \dot{\mathbf{o}}\cdot\mathbf{o}^{\mathrm{T}}. \tag{4}$$

Integration of Eq. $(2)_2$ for each meso-1 element (crystallite) at each moment of deformation yields the meso-1 stress tensor $\boldsymbol{\sigma}$ (subscripts of crystallite numbers are omitted). Using the stresses $\boldsymbol{\sigma}$, the normal unit vector, and the unit vector of the slip direction, we find the meso-1 shear stresses $\tau^{(k)}$ acting in each kth slip system:

$$\tau^{(k)} = \mathbf{b}^{(k)}\mathbf{n}^{(k)} : \boldsymbol{\sigma}, \tag{5}$$

where $\mathbf{b}^{(k)}$ is the unit vector along the Burgers vector of an edge dislocation, and $\mathbf{n}^{(k)}$ is the unit normal to the plane of the kth slip system in the current configuration. As the response of the representative macrovolume, we use the Cauchy stress tensor $\boldsymbol{\Sigma}$ determined at each moment of deformation by averaging the stress tensor $\boldsymbol{\sigma}$ over the set of crystallites that make up the macroscopic representative volume.

The most significant mechanisms of microstructure evolution in the constructed model are as follows: slip of edge dislocations, nucleation of dislocations from Frank–Read sources, annihilation of dislocations of different signs in each slip system, and change in the dislocation barrier density on slip systems. At mesolevel 2, the average velocities of positive and negative dislocations $V_{\pm}^{(k)}$ are determined, depending on the magnitude of shear stresses $\tau^{(k)}$, temperature θ, the density of positive and negative dislocations $\rho_{+}^{(k)}, \rho_{-}^{(k)}$, and the barrier density $\rho_{\mathrm{bar}}^{(k)}$ on slip systems. The rate of change of critical shear stresses $\dot{\tau}_{\mathrm{c}}^{(k)}$ is additively decomposed into two components, depending respectively on the change of dislocation densities in slip systems $\dot{\tau}_{\mathrm{c\,dis}}^{(k)}$ and the change of barrier densities $\dot{\tau}_{\mathrm{c\,bar}}^{(k)}$. The system of equations describing the change in these meso-2 variables can be written in the general form as follows:

$$\begin{cases} V_{\pm}^{(k)} = \pm f_1(\tau^{(k)}, \tau_{\mathrm{c}\pm}^{(k)}, \theta, \rho_{\pm}^{(l)}, \rho_{\mathrm{bar}}^{(kl)})\operatorname{sgn}\tau^{(k)}, \\ \dot{\rho}_{\pm}^{(k)} = f_2(\tau^{(k)}, \tau_{\mathrm{c}\pm}^{(k)}, \theta, \rho_{\pm}^{(k)}, \rho_{\mathrm{bar}}^{(kl)}), \; l = \overline{1,12}, \\ \dot{\gamma}^{(k)} = (\rho_{+}^{(k)} V_{+}^{(k)} - \rho_{-}^{(k)} V_{-}^{(k)})|\mathbf{b}|^{(k)}, \\ \dot{\rho}_{\mathrm{bar}}^{(kl)} = f_3(\tau^{(k)}, \tau_{\mathrm{c}\pm}^{(k)}, \theta, \rho_{\pm}^{(k)}, \rho_{\mathrm{bar}}^{(kl)}), \\ \tau_{\mathrm{c}0\pm}^{(k)} = \tau_{\mathrm{c\,lat}}^{(k)}, \\ \dot{\tau}_{\mathrm{c}\pm}^{(k)} = \dot{\tau}_{\mathrm{c\,dis}\pm}^{(k)} + \dot{\tau}_{\mathrm{c\,bar}\pm}^{(k)}. \end{cases} \tag{6}$$

The average dislocation velocities $V_+^{(k)}, V_-^{(k)}$ play an important role in describing the microstructural evolution and determining the shear rates, while the velocities of opposite-sign dislocations of the same slip system may differ in magnitude. We took into account that dislocations of both signs can move in the same slip system and did it using the Orowan rate equation [33], which takes into account the motion of different-sign dislocations:

$$\dot{\gamma}^{(k)} = (\rho_+^{(k)} V_+^{(k)} - \rho_-^{(k)} V_-^{(k)}) |\mathbf{b}|^{(k)}, \tag{7}$$

where $|\mathbf{b}|^{(k)}$ is the magnitude of the Burgers vector.

The average dislocation velocities are determined from the following equations [34]:

$$\begin{cases} V_+^{(k)} = l^{(k)} \nu \exp\left(-\dfrac{\Delta G_{*\pm}^k}{k_B \theta} \right) \\ \qquad \times H(|\tau^{(k)}| - \tau_{c+}^{(k)}) \operatorname{sgn} \tau^{(k)}, \\ V_-^{(k)} = -l^{(k)} \nu \exp\left(-\dfrac{\Delta G_{*\pm}^k}{k_B \theta} \right) \\ \qquad \times H(|\tau^{(k)}| - \tau_{c-}^{(k)}) \operatorname{sgn} \tau^{(k)}, \end{cases} \tag{8}$$

$$\Delta G_{*\pm}^k = \frac{\Delta F_*}{1 + g|\tau^{(k)}| / \tau_{c\pm}^{(k)}}, \; l^{(k)} = \alpha \frac{1}{\sqrt{\beta \sum_{l=1}^{n} \rho_{bar}^{kl} + \delta \sum_{l=1}^{n} \rho^l}},$$

where $l^{(k)}$ is the mean free path of a dislocation in the kth slip system, ν is the Debye frequency, ΔG_*^k is the activation energy for the motion of dislocations (depending on the current state of the microstructure and the shear stress on slip systems), ΔF_* is the activation energy for the motion of dislocations, k_B is the Boltzmann constant, θ is the temperature, and H is the Heaviside function.

Frank–Read sources generating closed expanding dislocation loops are considered as intragranular sources of dislocations. In this work, the generation of dislocations is described by introducing Frank–Read sources whose density change is described by the following equation [25]:

$$\dot{\rho}_{src\pm}^{(k)} = \sum_{j=1}^{12} L \rho_{bar}^{(kj)} \rho_\pm^{(j)} \times \left[l^{(j)} \nu \exp\left(-\frac{\Delta G_{*\pm}^{(j)}}{k_B \theta} \right) H(|\tau^{(j)}| - \tau_{c\pm}^{(j)}) \right], \tag{9}$$

$$\rho_{0src\pm}^{(k)} = \rho_{0src},$$

where $\rho_{bar}^{(kj)}$ is the barrier density at the intersection of the kth and jth slip systems (where dislocations can be pinned and dislocation loops can be formed). The contribution of the sources activated when the actual shear stresses exceed the critical source activation stresses τ_{src} to the increase in dislocation densities is proportional to the actual density of Frank–Read sources [35]:

$$\dot{\rho}_{nuc\pm}^{(k)} = r_{av} \rho_{src\pm}^{(k)} \nu \left\langle \frac{|\tau^{(k)}|}{\tau_{src}} - 1 \right\rangle^p, \tag{10}$$

$$\tau_{src} = \frac{A \mu b}{2\pi L} \left(\ln \frac{L}{r_0} + B \right),$$

where r_{av} is the average loop radius, A, B, p are the dimensionless parameters of the material, μ is the shear modulus, L is the distance between obstacles in the source, r_0 is the minimum length of the pinned segment that can generate dislocation loops, b is the magnitude of the Burgers vector, and the operator $\langle \cdot \rangle$ denotes the Macaulay brackets ($\langle x \rangle = x H(x)$).

Annihilation of dislocations is possible if two dislocations of opposite signs lie in parallel slip systems and are closely spaced. Dislocation annihilation is most often observed in tests with alternate loading. Dislocations of different signs belonging to the same slip system are attracted. When dislocations are in parallel slip systems, they can climb towards each other and annihilate at a distance equal to or less than a critical distance h_{ann}. The number of annihilated dislocations per unit time is proportional to the swept volume (the areas swept by moving edge dislocations multiplied by h_{ann}). We describe annihilation using the following equation [36]:

$$\dot{\rho}_\pm^{(k)ann} = -h_{ann} \rho_+^{(k)} \rho_-^{(k)} \left| V_+^{(k)} - V_-^{(k)} \right|. \tag{11}$$

The formation and evolution of barriers are described using the barrier formation matrix R_{bar}^{kl}, in which the unit values at the intersection of row k and column l denote the numbers of slip systems involving split dislocations, which interact upon intersection with the formation of Lomer–Cottrell or Hirt locks; all other components of the matrix R_{bar}^{kl} are zero. The rate of change in the barrier density depends on the dislocation density on the reacting systems, the actual shear stresses, and temperature [37]:

$$\dot{\rho}_{bar}^{(kl)} = \alpha x_d \sum_{l=k+1}^{K-1} \left[R_{bar}^{kl} \rho_\pm^{(k)} \rho_\pm^{(l)} (V_\pm^{(k)} + V_\pm^{(l)}) \right], k = \overline{1, K},$$

$$\dot{\rho}_{bar}^{(lk)} = \dot{\rho}_{bar}^{(kl)}, l = \overline{k+1, K-1}, k = \overline{1, K}, \tag{12}$$

$$x_d = \frac{b}{8\pi \varepsilon_{SFE}} = \frac{b^2 G}{8\pi \gamma_{SFE}},$$

where K is the number of slip systems, α is a dimensionless parameter, x_d is the average dislocation splitting width, and $\varepsilon_{SFE} = \gamma_{SFE}/(Gb)$ is the dimensionless

stacking fault energy γ_{SFE}. The matrix of barrier densities on slip systems contains data about all barriers (24 for fcc) that can form on split dislocations. The components of the matrix $\dot{\rho}_{bar}^{(kl)}$ describe the rates of change in barrier densities at the intersections of slip systems with numbers k and l.

The hardening law is formulated under the hypothesis of additivity of the critical stresses of slip systems and their rates of change due to contributions from the lattice resistance (a quantity that depends only on temperature) $\tau_{c\,lat}^{(k)}$, dislocation stress fields $\tau_{c\,dis\pm}^{(k)}$, and barriers formed on split dislocations $\tau_{c\,bar\pm}^{(k)}$ (k is the slip system number). The interaction of dislocations is evaluated using the known solution for a single dislocation in an isotropic elastic medium [38]. Based on this solution, we constructed the matrix M^{ki} to estimate the interaction stresses between dislocations of the kth and ith slip systems, which are entered at the intersection of the kth row and ith column of the matrix M^{ki}. By introducing a barrier on split dislocations as a set of two partial and sessile dislocations, we evaluated the effect of the barrier on the strengthening of the kth slip system due to the barrier on the ith slip system. This effect is described using the matrix B^{ki}. With the introduced matrices, evolution equations for changes in the critical shear stress and its components can be written as [39]:

$$\tau_{c0\pm}^{(k)} = \tau_{c\,lat}^{(k)},$$

$$\dot{\tau}_{c\pm}^{(k)} = \dot{\tau}_{c\,dis\pm}^{(k)} + \dot{\tau}_{c\,bar}^{(k)},$$

$$\dot{\tau}_{c\,dis\pm}^{(k)} = \alpha b \tau_{c0}^{(k)} \sum_{i=1}^{K} \frac{M^{ki}}{2\sqrt{\rho_{\pm}^{(i)}}} \dot{\rho}_{\pm}^{(i)}, \sum_{k}, \qquad (13)$$

$$\dot{\tau}_{c\,bar}^{(k)} = \beta b \tau_{c0}^{(k)} \sum_{i=1}^{n} \frac{B^{ki}}{2\sqrt{\rho_{bar}^{(ki)}}} \dot{\rho}_{bar}^{(ki)}, \sum_{k},$$

where α, β are the dimensionless parameters of the material.

3. ALGORITHM FOR THE NUMERICAL IMPLEMENTATION OF THE MODEL

The proposed model for describing the response of a representative macrovolume (macroscopically homogeneous sample) can be implemented by the following algorithm. Since the problem (geometric and physical) is highly nonlinear, it is solved using a step-by-step loading procedure: the entire considered time interval is represented by a set of time steps, and the length of the steps is determined from numerical experiments under the specified condition for convergence of results. Prior to calculations, the necessary initial conditions and material parameters are set for the variables of all levels. It is assumed that the material in the initial state is in its natural configuration. The loading is induced kinematically. The macroscopic velocity gradient $\hat{\mathbf{\nabla}}\mathbf{V}(t)$ and the temperature are considered to be given as continuous tensor- and scalar-valued functions of time t, respectively. Note that when using the model to analyze the deformation of specific structural elements, the impact parameters at each point of time are determined from the solution of the corresponding boundary value problems.

At each time step, the kinematic and thermal effects specified at the macrolevel are transferred to mesolevel 1. The solution of the problem yields the values of all internal variables at mesolevels 1 and 2, including explicit ones, i.e., included in the constitutive equations of a given level. The internal variables of these levels are listed and classified in Table 1. Note that the response of the representative macrovolume of a material (macroscopic Cauchy stress tensor $\mathbf{\Sigma}$) is determined by averaging the mesoscopic stresses $\boldsymbol{\sigma}$, and therefore there is no need for a macroscopic constitutive equation.

The constitutive relations of mesolevel 2 are the equation for determining the shear rates on slip systems from the dislocation densities and velocities. Loading at the macrolevel and mesolevel 1 at each time step is given by the velocity vector gradient. The loads at mesolevel 2 are the stresses determined at the end of the previous step in meso-1 elements. The algorithm for solving the problem at mesolevels 1 and 2 for each time step consists of three stages.

1. Solution in terms of rates. The temperature and the velocity gradient set at the macrolevel are transferred to mesolevel 1 (using Voigt's hypothesis). The stress tensor components determined at the end of the previous time step are used to determine the shear stresses in each meso-1 element (Eq. (5)). Then we calculate the rates of change in the internal variables of meso-2 elements, including the dislocation densities and velocities, which are then used to calculate the shear rates on slip systems and the inelastic part of the strain rate. The latter are transferred to mesolevel 1, where the rates of stress change are determined.

Table 1. The list and classification of internal variables of mesolevels 1 and 2

Level	Type of internal variables	Designation	Name	Determination method
Meso 1	Explicit	$\mathbf{z}^{\text{in}}$	Inelastic part of the strain rate	Component of the load on meso-1 elements
Meso 1	Explicit	$\boldsymbol{\pi}$	Elastic moduli tensor (4th rank)	Determined by single crystal properties and lattice orientation $\mathbf{o}$
Meso 1	Explicit	$\boldsymbol{\omega}$	Spin tensor (meso 1)	Determined for each crystallite at each step
Meso 1	Implicit	$\mathbf{o}$	Lattice orientation tensor	Determined by integration over $\boldsymbol{\omega}$
Meso 1 Meso 2	Implicit Explicit	$\dot{\gamma}^{(k)}$	Shear rates on the kth slip system	Determined from dislocation velocities and densities at meso 2
Meso 1 Meso 2	Implicit Explicit	$\tau^{(k)}$	Shear stresses on the kth slip system	Determined by $\boldsymbol{\sigma}$, load on meso 2
Meso 2	Explicit	$V_{\pm}^{(k)}$	Average dislocation velocities on the kth slip system	Determined by $\tau^{(k)}, \tau_{c\pm}^{(k)}$, and θ
Meso 2	Explicit	$\rho_{+}^{(k)}, \rho_{-}^{(k)}$	Dislocation densities (+ / –) on the kth slip system	Determined from evolution equations
Meso 2	Implicit	$\rho_{\text{bar}}^{(k)}$	Barrier densities on the kth slip system	Determined from evolution equations
Meso 2	Implicit	$\tau_{c\pm}^{(k)}$	Critical stress values on the kth slip system	Sum of $\tau_{c\,\text{dis}}^{(k)}$ and $\tau_{c\,\text{bar}}^{(k)}$
Meso 2	Implicit	$\tau_{c\,\text{dis}\pm}^{(k)}$	Critical stresses on the kth slip system (dislocation-induced)	Determined by $\rho_{+}^{(k)}, \rho_{-}^{(k)}$
Meso 2	Implicit	$\tau_{c\,\text{bar}}^{(k)}$	Critical stresses on the kth slip system (barrier-induced)	Determined by $\rho_{\text{bar}}^{(k)}$
Meso 2	Implicit	θ	Temperature	Impacts

2. Integration. All variables (including internal variables) at all levels are determined by integrating their rates of change at the end of the current time step and at the beginning of the next one.

It should be noted that in the first and second stages of the calculations, the meso-1 and meso-2 tensor parameters are determined by the components in the bases of the rigid corotational frames of this level (recall that meso 1 and meso 2 belong to the same scale level).

3. Redetermination of internal variables. Using the spins of the corotational frames determined at the first stage, we determine the changes in the orientations of meso-1 and meso-2 elements and redefine the tensor variables of these levels at the end of the considered time step (binding the calculated tensor components to the changed basis vectors of crystallites). The stress tensor components in the basis of the background frame of reference are calculated and averaged to estimate the macroscopic stress tensor components.

4. APPLICATION OF THE MODEL TO DESCRIBE PROPORTIONAL AND NONPROPORTIONAL CYCLIC DEFORMATION

The developed model was applied to describe the response of fcc polycrystalline macrosamples subjected to proportional and nonproportional cyclic loading. The representative macrovolume (macrosample) was assumed to consist of 343 crystallites with the distribution of their orientations in the reference configuration according to a uniform law. Numerical experiments were carried out on model representative volumes of brass (60% Cu, 40% Zn) and pure aluminum, which have different values of the components of the tensor of elastic properties, initial lattice resistance, stacking fault energy (155 mJ/m^2 for aluminum, 50 mJ/m^2 for brass), and hardening law parameters. The initial dislocation densities are assumed to be the same and equal to 10^9 cm^{-2}. The initial barrier densities are zero.

Loading in the considered numerical experiments is induced kinematically. Two loading programs

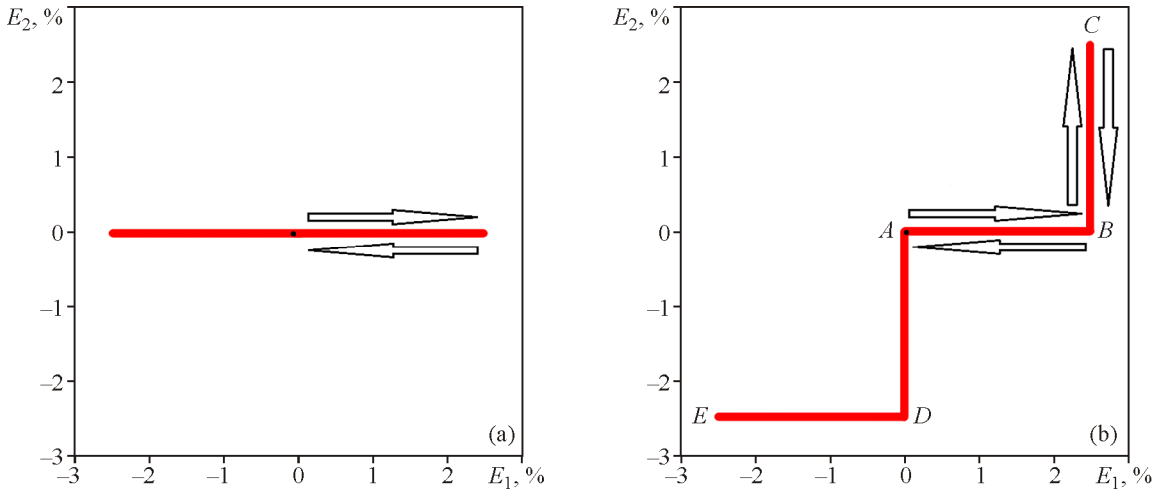

Fig. 2. Loading programs: simple tension/compression (a) and stepped loading along the path *A-B-C-B-A-D-E-D* (two steps) (b) in a two-dimensional subspace of Ilyushin's five-dimensional strain space.

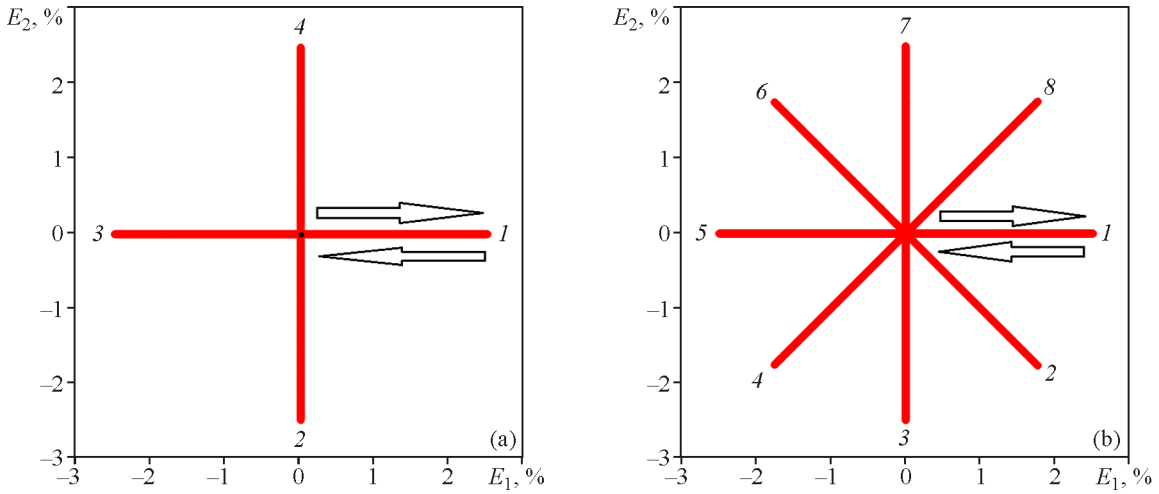

Fig. 3. Loading programs with radial paths in a two-dimensional subspace of Ilyushin's five-dimensional strain space, 4 (a) and 8 rays (b).

are considered: proportional and nonproportional. Deformations are limited by maximum equivalent strain amplitudes. The main purpose of the study is to analyze the differences in the response of the materials under different loading programs, which are observed in full-scale experiments [40–44]. At small displacement gradients, lattice rotations in crystallites can be neglected and the loading can be specified in terms of small strains and strain rates. Kinematic loads are given by vector components in Ilyushin's five-dimensional strain vector space. Proportional loading was described by specifying one vector component, and for nonproportional loading we specified the time dependences of two strain vector components (Figs. 2–4).

The results of numerical cyclic loading tests on brass and aluminum macrosamples along a rose-shaped path are shown in Fig. 5.

It is of most interest to describe the additional hardening effect, i.e., an increase in the equivalent stress amplitude under nonproportional loading in comparison with proportional cyclic loading at the same equivalent strain amplitudes. Using the specified kinematic loads, we determined the maximum equivalent stresses (after reaching stationary values in the curve of stress amplitude versus accumulated strain). To evaluate the amount of additional hardening in terms of the obtained maximum equivalent stresses, we subtracted from them the maximum equivalent stresses obtained in proportional cyclic loading tests

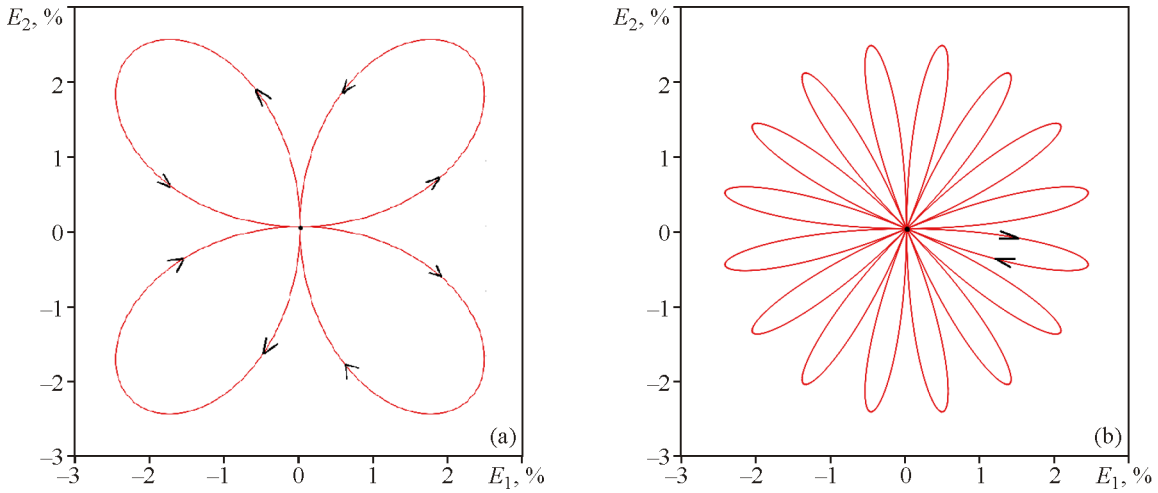

Fig. 4. Loading programs with rose-shaped paths in a two-dimensional subspace of Ilyushin's five-dimensional strain space, 4 (a) and 16 petals (b) (color online).

(also after the curve reached a stationary value) and referred to the latter, thus determining the amount of additional hardening as a percentage of the reference value. Data on the relationship between the amount of additional hardening and the loading program are presented in Table 2.

Numerical experiments showed that additional hardening is more pronounced in the material with low stacking fault energy (brass) for the same loading programs. The dependence of stress amplitude on accumulated strain reaches a stationary value on average at 45% accumulated strain. In this case, the dislocation densities increase by 4-5 orders of magnitude, depending on the complexity of loading. In the brass sample, the increase in the flow stress is significantly contributed by hardening due to the formation

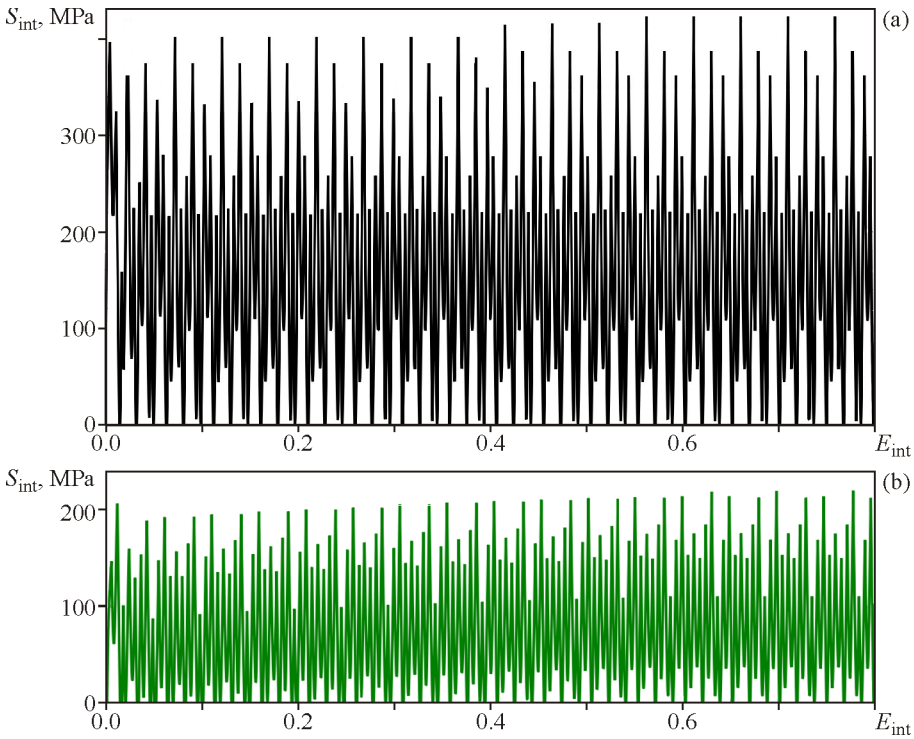

Fig. 5. Dependence of stress amplitudes on accumulated strains in brass (a) and aluminum samples (b) under cyclic loading along rose-shaped paths in a two-dimensional subspace of Ilyushin's five-dimensional space, 4 petals (color online).

Table 2. Additional hardening of polycrystalline aluminum and brass samples for various loading programs

Loading program	Additional hardening, %		Stress amplitudes in stationary mode, MPa	
	Aluminum	Brass	Aluminum	Brass
Tension/compression	0.0	0.0	207.1	312.3
Stepped, 2 steps	0.6	5.1	208.4	328.1
Stepped, 4 steps	0.8	5.3	208.8	329.0
Radial, 4 rays	1.0	4.9	209.1	327.5
Radial, 8 rays	1.8	5.3	210.8	328.9
Radial, 16 rays	2.0	5.6	211.2	329.7
Rose-shaped, 4 petals	12.6	31.8	233.1	411.6
Rose-shaped, 8 petals	14.5	35.9	237.2	424.4
Rose-shaped, 16 petals	15.3	37.5	238.8	429.5

of barriers on split dislocations. The qualitative agreement of the calculation results to the experimental data reported in [40, 41] suggests that the developed model is in principle applicable for describing the cyclic, including nonproportional, loading of materials with different stacking fault energies.

5. CONCLUSIONS

The structure and mathematical formulation of a three-level dislocation-based model for describing the deformation of polycrystalline samples under variable kinematic loading programs were considered. The main focus in the development of the model was on describing the defect density evolution and barrier formation on split dislocations. The model explicitly describes the behavior of arrays of perfect and split dislocations on slip systems, which allows one to describe in detail the deformation and hardening mechanisms of materials subjected to arbitrary deformation paths.

The proposed model was applied to describe proportional and nonproportional cyclic deformation of fcc polycrystalline samples with significantly different stacking fault energies. It was shown that materials with low stacking fault energy under nonproportional cyclic loading demonstrate more pronounced additional cyclic hardening compared to materials with high stacking fault energy.

FUNDING

The work was carried out with financial support from the Ministry of Science and Higher Education of the Russian Federation (as basic part of the government statement of work for PNRPU, Project No. FSNM-020-0027) and the Russian Foundation for Basic Research (Project No. 20-41-596002 r (Perm Scientific and Educational Center)).

REFERENCES

1. Ilyushin, A.A., *Plasticity: Fundamentals of General Mathematical Theory*, Moscow: AN SSSR, 1963.
2. Sokolovskii, V.V., *Theory of Plasticity*, Moscow: Vyssh. Shkola, 1969.
3. Malinin, N.N., *Applied Theory of Plasticity and Creep*, Moscow: Mashinostroenie, 1968.
4. Kachanov, L.M., *Foundations of the Theory of Plasticity*, North-Holland Pub. Co., Amsterdarm, 1971.
5. Pozdeev, A.A., Trusov, P.V., and Nyashin, Yu.I., *Large Elastoplastic Deformations: Theory, Algorithms, Applications*, Moscow: Nauka, 1986.
6. Laird, C., Charsley, P., and Mughrabi, H., Low Energy Dislocation Structures Produced by Cyclic Deformation, *Mater. Sci. Eng*., 1986, vol. 81, pp. 433–450.
7. Vasin, R.A., Constitutive Relations in the Theory of Plasticity, *Itogi Nauk. Tekhn. Mekh. Deform. Tv. Tela. VINITI*, 1990, vol. 21, pp. 3–75.
8. Doquet, V., Twinning and Multiaxial Cyclic Plasticity of a Low Stacking-Fault-Energy F.C.C. Alloy, *Acta Metall. Mater.*, 1993, vol. 41, pp. 2451–2459.
9. Rogovoy, A.A., *Formalized Approach to the Construction of Solid Mechanics Models. Part 1. Basic Equations of Continuum Mechanics*, Moscow: Institute of Computer Science, 2021.
10. Taylor, G.I., Plastic Strain in Metals, *J. Inst. Met*., 1938, vol. 62, pp. 307–324.
11. Bishop, J.F. and Hill, R., A Theory of the Plastic Distortion of a Polycrystalline Aggregate under Combined Stresses, *Philos. Mag. Ser. 7*, 1951, vol. 42, no. 327, pp. 414–427. https://doi.org/10.1080/14786445108561065

12. Bishop, J.F.W. and Hill, R., A Theoretical Derivation of the Plastic Properties of a Polycrystalline Face-Centered Metal, *Philos. Mag. Ser. 7*, 1951, vol. 42, no. 334, pp. 1298–1307. https://doi.org/10.1080/14786444108561385
13. *Physical Mesomechanics of Heterogeneous Media and Computer-Aided Design of Materials*, Panin, V.E., Ed., Cambridge: Cambridge Interscience Publishing, 1998.
14. Krivtsov, A.M., *Deformation and Fracture of Solids with Microstructure*, Moscow: FIZMATLIT, 2007.
15. Horstemeyer, M.F., Multiscale Modeling: A Review, in *Practical Aspects of Computational Chemistry*, Leszczynski, J. and Shukla, M.K., Eds., Heidelberg: Springer, 2009, pp. 87–135. https://doi.org/10.1007/978-90-481-2687-3_4
16. Roters, F., *Advanced Material Models for the Crystal Plasticity Finite Element Method: Development of a General CPFEM Framework*, Aachen: RWTH Aachen, 2011.
17. Li, P., Li, S.X., Wang, Z.G., and Zhang, Z.F., Fundamental Factors on Formation Mechanism of Dislocation Arrangements in Cyclically Deformed FCC Single Crystals, *Progr. Mater. Sci*., 2011, vol. 56, pp. 328–377. https://doi.org/10.1016/J.PMATSCI.2010.12.001
18. Cho, J., Molinari, J.-F., and Anciaux, G., Mobility Law of Dislocations with Several Character Angles and Temperatures in FCC Aluminum, *Int. J. Plasticity*, 2017, vol. 90, pp. 66–75. https://doi.org/10.1016/j.ijplas.2016.12.004
19. Romanova, V.A., Balokhonov, R.R., Batukhtina, E.E., Emelyanova, E.S., and Sergeev, M.V., On the Solution of Quasi-Static Micro- and Mesomechanical Problems in a Dynamic Formulation, *Phys. Mesomech*., 2019, vol. 22, no. 4, pp. 296–306. https://doi.org/10.1134/S1029959919040052
20. Bisht, A., Kumar, L., Subburaj, J., Jagadeesh, G., and Suwas, S., Effect of Stacking Fault Energy on the Evolution of Microstructure and Texture during Blast Assisted Deformation of FCC Materials, *J. Mater. Process. Technol*., 2019, vol. 271, pp. 568–583. https://doi.org/10.1016/j.jmatprotec.2019.04.029
21. Liang, Q., Weng, S., Fu, T., Hu, S., and Peng, X., Dislocation Reaction-Based Formation Mechanism of Stacking Fault Tetrahedra in FCC High-Entropy Alloy, *Mater. Chem. Phys*., 2022, vol. 282, p. 125997. https://doi.org/10.1016/j.matchemphys.2022.125997
22. McDowell, D.L., A Perspective on Trends in Multiscale Plasticity, *Int. J. Plasticity*, 2010, vol. 26, pp. 1280–1309. https://doi.org/10.1016/j.ijplas.2010.02.008
23. Beyerlein, I. and Knezevic, M., Review of Microstructure and Micromechanism-Based Constitutive Modeling of Polycrystals with a Low-Symmetry Crystal Structure, *J. Mater. Res*., 2018, vol. 33, pp. 3711–3738. https://doi.org/10.1557/jmr.2018.333
24. Trusov, P.V. and Shveikin, A.I., *Multilevel Models of Single- and Polycrystalline Materials: Theory, Algorithms, Application Examples*, Novosibirsk: Izd-vo SO RAN, 2019.
25. Trusov, P.V. and Gribov, D.S., The Three-Level Elastoviscoplastic Model and Its Application to Describing Complex Cyclic Loading of Materials with Different Stacking Fault Energies, *Materials*, 2022, vol. 15(3). https://doi.org/10.3390/ma15030760
26. Coleman, B.D. and Gurtin, M.E., Thermodynamics with Internal State Variables, *J. Chem. Phys*., 1967, vol. 47, pp. 597–613. https://doi.org/10.1063/1.1711937
27. Rice, J.R., Inelastic Constitutive Relations for Solids: An Internal-Variable Theory and Its Application to Metal Plasticity, *J. Mech. Phys. Solids*, 1971, vol. 19, pp. 433–455. https://doi.org/10.1016/0022-5096(71)90010-X
28. Maugin, G.A., *Mechanics of Electromagnetic Solids*, Norwell: Kluwer Academic Publishers, 2003.
29. Ashikhmin, V.N., Volegov, P.S., and Trusov, P.V., Constitutive Equations with Internal Variables: General Structure and Application to Texture Formation in Polycrystals, *PNRPU Bull. Mat. Modelir. Sistem Protsess.*, 2006, no. 14, pp. 11–26.
30. Trusov, P.V. and Shveikin, A.I., *Theory of Plasticity*, Perm: Izd-vo PNRPU, 2011.
31. Maugin, G.A., The Saga of Internal Variables of State in Continuum Thermo-Mechanics (1893–2013), *Mech. Res. Commun*., 2015, vol. 69, pp. 79–86. https://doi.org/10.1016/j.mechrescom.2015.06.00
32. Trusov, P.V. and Shveykin, A.I., On Motion Decomposition and Constitutive Relations in Geometrically Nonlinear Elastoviscoplasticity of Crystallites, *Phys. Mesomech*., 2017, vol. 20, no. 4, pp. 377–391. https://doi.org/10.1134/ S1029959917040026
33. Orowan, E., Problems of Plastic Gliding, *Proc. Phys. Soc*., 1940, vol. 52, pp. 1926–1948. https://doi.org/10.1088/0959-5309/52/1/303
34. Kocks, U.F., Constitutive Behavior Based on Crystal Plasticity, in *Unified Constitutive Equations for Creep and Plasticity*, Miller, A.K., Ed., Dordrecht: Springer, 1987, pp. 1–88. https://doi.org/10.1007/978-94-009-3439-9_1
35. Orlov, A.N., *Introduction to the Theory of Defects in Crystals*, Moscow: Vyssh. Shkola, 1983.
36. Arsenlis, A. and Parks, D.M., Modeling the Evolution of Crystallographic Dislocation Density in Crystal Plasticity, *J. Mech. Phys. Solids*, 2002, vol. 50, pp. 1979–2009. https://doi.org/10.1016/S0022-5096(01)00134-X
37. Shtremel, M.A., *Strength of Alloys. Part I. Lattice Defects*, Moscow: MISIS, 1999.
38. Cottrell, A.H., *Dislocations and Plastic Flow in Crystals*, Oxford University Press, New York, 1953.
39. Franciosi, P., The Concepts of Latent Hardening and Strain Hardening in Metallic Single Crystals, *Acta*

Metall., 1985, vol. 33, pp. 1601–1612. https://doi.org/10.1016/0001-6160(85)90154-3

40. Benallal, A. and Marquis, D., Effects of Non-Proportional Loadings in Cyclic Elasto-Viscoplasticity: Experimental, Theoretical and Numerical Aspects, *Eng. Comput*., 1988, vol. 5, pp. 241–247. https://doi.org/10.1108/eb023742
41. Benallal, A., Le Gallo, P., and Marquis, D., An Experimental Investigation of Cyclic Hardening of 316 Stainless Steel and of 2024 Aluminium Alloy under Multiaxial Loadings, *Nucl. Eng. Design*, 1989, vol. 114, pp. 345–353. https://doi.org/10.1016/0029-5493(89)90112-x
42. Xia, Z. and Ellyin, F., Nonproportional Multiaxial Cyclic Loading: Experiments and Constitute Modeling, *J. Appl. Mech*., 1991, vol. 58, pp. 317–325. https://doi.org/10.1115/1.2897188
43. Aubin, V., Quaegebeur, P., and Degallaix, S., Cyclic Behaviour of a Duplex Stainless Steel under Multiaxial Loading: Experiments and Modelling, *Eur. Struct. Integr. Soc*., 2003, vol. 31, pp. 401–422. https://doi.org/10.1016/S1566-1369(03)80022-5
44. Zhang, J. and Jiang, Y., An Experimental Investigation on Cyclic Plastic Deformation and Substructures of Polycrystalline Copper, *IJOP*, 2005, vol. 21, pp. 2191–2211. https://doi.org/10.1016/j.ijplas.2005.02.004